How to Cite:
Mohamed, A. R., Hussein, H. H., & Sirhan, M. M. (2022). Removal lead (II) and chromium (III) Ions from aqueous solutions, by copper nanoparticles prepared using Capparis spinosa leaf extract. *International Journal of Health Sciences*, *6*(S4), 9091–9106. https://doi.org/10.53730/ijhs.v6nS4.11900

Removal lead (II) and chromium (III) Ions from aqueous solutions, by copper nanoparticles prepared using Capparis spinosa leaf extract

Ahmed R Mohamed
Department of Chemistry, College of Education for Pure Sciences, University of Anbar, Ramadi, Iraq
Corresponding author email: ahm20u4138@uoanbar.edu.iq

Hanaa H. Hussein
Department of Chemistry, College of Science, Mustansiriyah University, Baghdad, Iraq
Email: albajalanhanaa@uomustansiriyah.edu.iq

M. M. Sirhan
Department of Chemistry, College of Education for Pure Sciences, University of Anbar, Ramadi, Iraq
Email: albajalanhanaa@yahoo.com

***Abstract*---**The manufacture of copper oxide nanoparticles utilizing a green method is the subject of the study (environmentally friendly). The Capparis Spinosa plant's aqueous extract was used. The adsorption batch method was used to extract Pb (II) and Cr (III) ions from their aqueous solutions using this oxide. To describe and study the surface FT-IR, XRD, SEM, TEM, and AFM were among the methods used. were applied. All of the reflection peaks with relative intensities of different planes, as determined by XRD analysis, indicate CuO was found, and the spectral analysis revealed that the particle size produced was about (14.28 nm), which corresponded to those estimated by SEM and TEM. The sizes of the CuO particles were measured using SEM, TEM, and AFM, and they were found to be in the nanoscale range. The result of the impact of contact time, adsorbent dose, introductory fixation Finally, the thermodynamic bounds for the impact of temperature were calculated after considering pH and temperature.

***Keywords*---**adsorption, decontamination, nanoparticle, green chemistry.

Introduction

Nanotechnology has been increasingly essential in the present period of study (Furno et al., 2004). This technology could be used in a variety of sectors, including medicine, pharmaceuticals, nutrition, chemistry, energy research, and cosmetics. Furthermore, it has some use in alternative medicine (Basarkar & Singh, 2009; Brigger et al., 2012; Roy et al., 1999; Wilson et al., 2010). Green chemistry is the creation and development of chemical goods and processes with the goal of reducing harmful environmental uses (Priya et al., 2011). Chemical and physical ingredients are used to make nanoparticles. Green synthesis was one of the best approaches for creating nanoparticles when compared to various methods. Green synthesis has gained popularity in recent years due to its cost-effectiveness, ability to employ low temperatures and non-toxic ingredients, and compatibility with a wide range of materials. applications, for example, clinical and wholesome projects (Tagad et al., 2013).

A green union strategy is being created which is additionally a harmless to the ecosystem technique (Ezhilarasan et al., 2011). In this strategy the watery plant extricate is utilized as a diminishing specialist to set up the nanostructures. In light of the electrical, optical and invigorating properties, copper nanoparticles are generally utilized and have numerous clinical, modern, antifungal and antibacterial applications (Awwad & Salem, 2012; Jagtap & Bapat, 2013). The green synthesis approach has been utilized to produce nanoparticles from a variety of plants (Safarpour et al., 2012). All components of the plant, including the stem, flower, fruit, leaves, and bark, are used to make nanoparticles (Mallikarjuna et al., 2011). Capparis Spinosa is the largest genus in the Capparis Spinosa family of flowering, angiosperm, dicotyledonous plants (Zargari, 1988). Capparis Spinosa is its scientific name. There are various names for it, including. This plant is a shrub with 8 to 15 leaf stems that are evenly spaced (Ghahraman, 1994). The leaves of this plant were employed to produce copper nanoparticles and test their ability to adsorb heavy ions from water in the current investigation. Because copper oxide nanoparticles have key qualities including high efficiency and low cost, researchers are more interested in using them to remove heavy metals from polluted water. Adsorption efficiency and bigger active sites appear to be advantages of nanoparticles (Devi & Singh, 2014). The most essential and popular nanoparticle fabrication techniques are sol-gel, vapor deposition, electrochemical method, combustion, colloidal thermosynthesis process, microwave irradiation, thermal oxidation, pulse wire blast methods, deposition, and colloidal solution gel (Ahamed et al., 2014; Luna & Commission, 2015; Phiwdang et al., 2013). This study's green method methodology is one of the most essential and widely utilized nanoparticle production techniques (Mahdi, 2013).

Methods and Materials

Absorbance

Pb (NO3)2 and CrCl2.H2O in deionized water were used to make standard stock solutions of Pb (II) and Cr (III) ions (1000 ppm). From this standard stock of each metal ion, several concentrations (10, 20, 30, 40, 50, 60, and 70 ppm) were created. To assess the amounts of metals by atomic absorption, the absorbance of

these solutions was measured at a wavelength (max) of 458 nm for Pb (II) and 488 nm for Cr (III).

Set the calibration curve

To determine the calibration curve for each of the ternary lead ion (Pb+2) and chromium ion (Cr+3), a series of standard solutions with multiple concentrations (5, 15, 25, 35 ppm) were prepared for each of (Pb+2) and chromium ion (Cr +3) Then, the absorbance was measured at the greatest wavelength of each model, which is (217nm) for the lead ion (pb+2) and (357nm) for the chromium ion (Cr+3). Through the application of Beer-Lamberts Law, which represents the relationship between absorbance and concentration, and through the obtained values, the standard calibration curve for each model was obtained, as shown in the figures below:

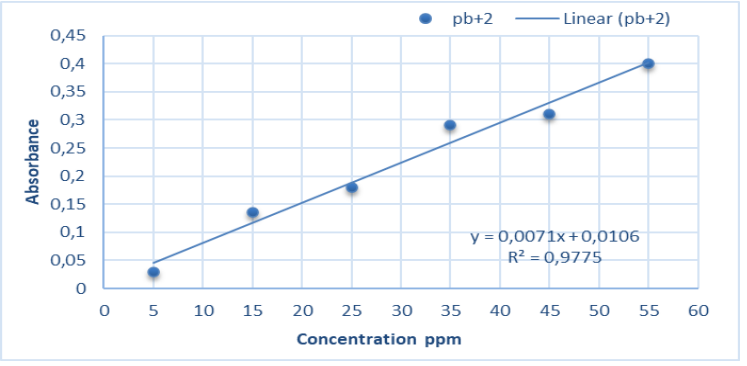

Figure 1. Standard Calibration Curve for Lead Ion (pb^{+2})

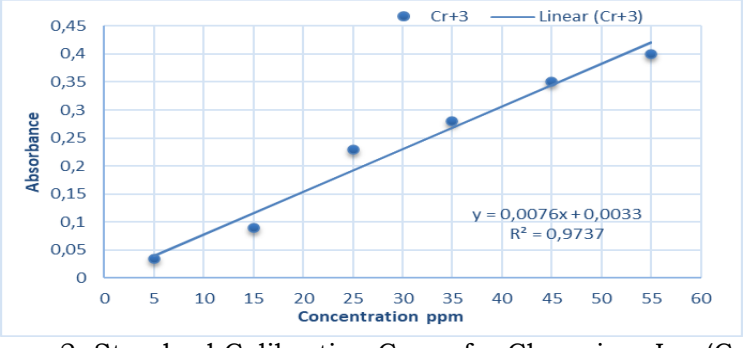

Figure 2. Standard Calibration Curve for Chromium Ion (Cr^{+3})

Preparation of the plant extract, not the leaves, Capparis Spinosa

The plant extract of spindle capris leaves was prepared by collecting Capparis Spinosa leaves from one of the villages of Al-Baghdadi district. Then the dry leaves are ground with a mortar, then ground by an electric mill to obtain a fine powder, and then sieved with a sieve with a diameter (212 nm) to get rid of residual impurities and plankton, where the powder is kept in the shade away from light. (5 g) of the resulting powder was weighed into a (500 mL) glass beaker and (400 mL) deionized water was added. Taking into account the continuous

stirring by a magnetic stirrer, the mixture is heated to a temperature (80 ° C) for a full hour to obtain the brown-colored extract as shown in the figure (3) after cooling the extract to room temperature and filtered by filter papers to obtain a solution that we put in Test tubes and centrifuge at 1200 rpm for 5 minutes to get rid of residual fibers. Reducing agent (Do et al., 2019).

Figure 3. Aqueous extract no Capparis Spinosa

Preparation of Copper Oxide nanoparticle

Nano-copper oxide was prepared by the green method and using the previously prepared plant extract from capers leaves, where Copper nitrate (Cu (NO3)2) (0.6 g) was dissolved in (100 ml) of deionized water with continuous stirring. For 10 minutes at room temperature, then (20ml) of the plant extract was gradually added using the burette, where the color changed from blue to light yellow, and then the temperature was gradually raised to (80°C), where the pH was adjusted by adding (0.1M)) of sodium hydroxide (NaOH) in the form of drops until the pH was equalized and the solution became neutral (PH = 7) Where the color changed to brown, the solution was left to cool and then the filtrate was separated by a centrifuge, the filtrate was collected and washed with deionized water and absolute ethanol and dried at a temperature of (60°C) for three hours and the powder was kept at a low temperature (Do et al., 2019).

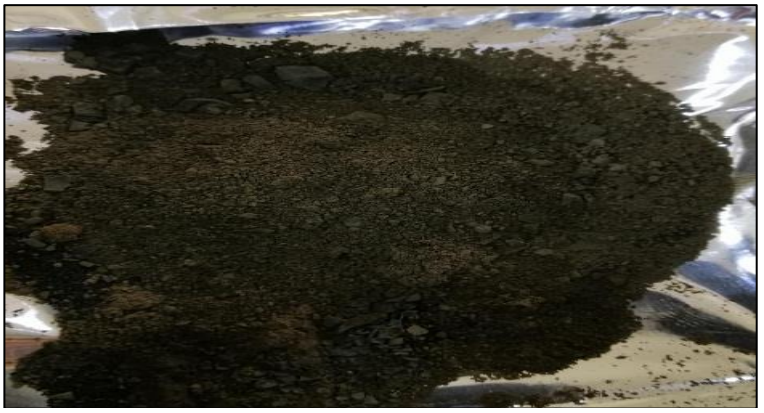

Figure 4. Nano-copper oxide prepared by the green method

Adsorption study

Several volumetric flasks were constructed, each containing 50 ml (5 ml) of (1000ppm) pb (II) and Cr(III) ion solution (45 ml) of distilled water (pH 6), and (0.05g) of the pre-made (CuO.NP). At varied intervals of 15, 30, 45, 60, 75, 90, 105, and 120 minutes, the beaker was placed in a (water-bath mixing equipment) at 150 rpm and room temperature (298 K). The concentrations of the metal solution were determined by atomic absorption, and the effects of contact time, initial concentration, amount of adsorbent, pH, and temperature on the adsorption of the two metals on (CuO NPs) were investigated. Using the equation below (Onundi et al., 2010; Rozaini et al., 2010), the percentage of time spent removing the two metals was computed.

$$R\ \% = \frac{Co - Ce * 100}{Co}$$

Where (R percent) is the percentage of metals removed, (Co) is the initial concentration of metal ions (in binary system) (mg/L), and (Ce) is the concentration of Lead ions after removal (mg/L).

Adsorption isotherm experiment

Isotherm of adsorption to remove Pb+2 and Cr+3 ions in (CuO NPs) at 25°C, pH (6.5), 0.05g of adsorbent For any metal on a ready surface, use a stirring speed of 150 rpm and a contact time of 60 minutes. (50 ml),concentration of Pb (II) and Cr (III) solution was given. Complete Experiments (AAS) proved that the adsorption sample is: It was calculated by the following equation (Onundi et al., 2010; Rozaini et al., 2010).

$$Qe = \frac{(C_o - Ce) * v}{m}$$

Where (Qe) is the equilibrium adsorption quantity of surface nanoparticles (mg/g), and (Co) is the initial adsorbent concentration (mg/L). (Ce), metal adsorption equilibrium concentration (mg/L), (V), volume of aqueous solution (L), (m), weight of metal oxide nanoparticles (g).

Discussion and Results

XRD analysis of CuO-NPs

Figure (5) shows the XRD pattern of CuO NPs CuO Nano powder has a highly crystalline structure, as evidenced by the existence of distinct and sharp peaks with various 2 values (Manjari et al., 2017; Prasad et al., 2017). The monoclinic phase of CuO (JCPDS01-080-1268) can be indexed by the examination of assigned crystal planes (Bragg reflection) of very significant peaks (Buazar et al., 2019; Wang et al., 2002). The green CuO NPs had no additional peaks on the XRD pattern, indicating that they were thoroughly purified. CuO NPs with the greatest peak at 2 theta = 35.60° (111) had a crystal size of 15.71 nm, according to the Debye-Scherer formula. At 2 theta= 38.93° (022), the wavelength was

measured to be 14.28 nm. These diffraction planes were very close to the data in the literature (Bedi & Singh, 2010). Size of the average crystallite

$$D = \frac{0.9\lambda}{\beta cos\theta}$$

Where (D) denotes the crystallite size, (λ) the radiation wave length, (θ) the Bragg's angle, and (β) the full width at half maximum (FWHM). The particle size of the (CuO.NPs) that was discovered is (14.28 nm). The presence of strong peaks in XRD samples and particle sizes smaller than 100 nm indicates that the surface is nanocrystalline.

Table 1
The strongest three peaks in XRD of (CuO-NPs)

No	2θ (deg)	dĂ	FWHM- (deg)	Intensity (counts)
1	32.9137	3.63437	2.9369	976
2	35.6009	2.52304	0.5313	578
3	38.9343	2.26853	0.4616	492

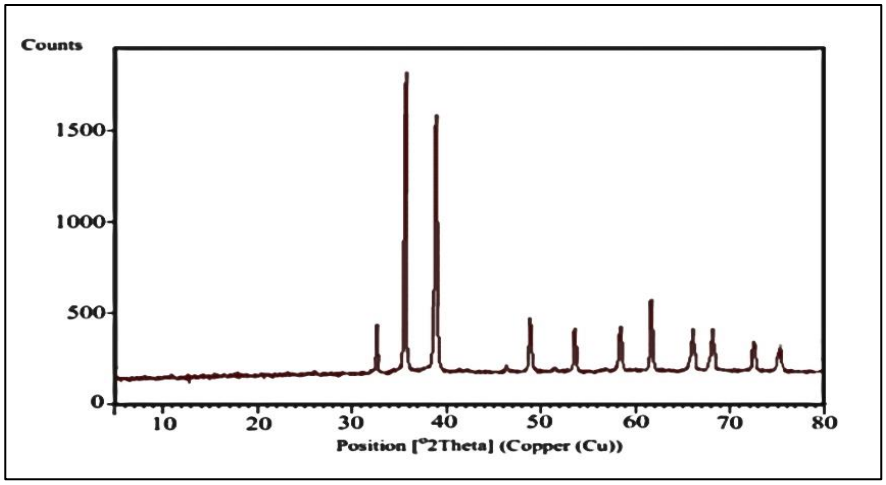

Figure 5. XRD patterns of (CuO-NPs) produced by Capparis Spinosa extract

FT-IR analysis of CuO NPs

The stretching vibration of the C-OH band from proteins amide of leaves extract can be assigned to the bands at1589.34 and 1415.75 cm-1. Peaks in the area 1307.74, 1091.72cm-1 can be attributable to carboxylic acid and amino group stretching vibrations. Aromatic compounds residue in caper leaf aqueous extract was attributed to the band at 6013.36 cm-1 Copper oxide nanoparticles FT-IR analysis Attributed to the presence of Cu-O nanoparticles fig(6) showed strong peaks at 470.63 and 451.34cm-1 (Bordbar et al., 2017; Ijaz et al., 2017).

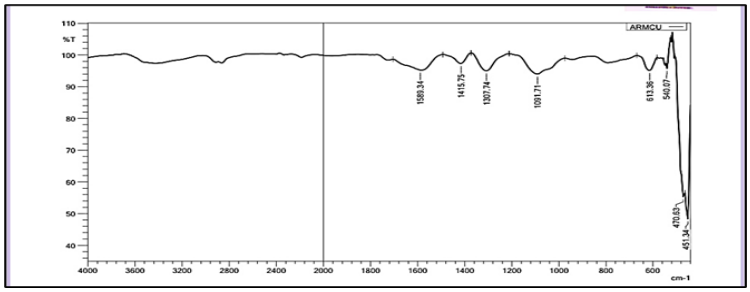

Figure 6. FT-IR analysis of (CuO-NPs).

Scanning electron Microscope (SEM)

A scanning electron microscope (SEM) called an AIS2300C was utilized to image the nanoparticles. A scanning electron microscope was used to analyze the morphology (SEM) (Sutradhar et al., 2014; Topnani et al., 2010). The appearance and size of green generated CuO-NPs" produced from caper leaves aqueous extract were determined by SEM examination. The green CuO NPs have a bacillary morphology, with an agglomeration of tiny particles that emerge in cluster form, as illustrated in Fig 7. The size range of the green synthesized CuO-NPs is 30–40nm.

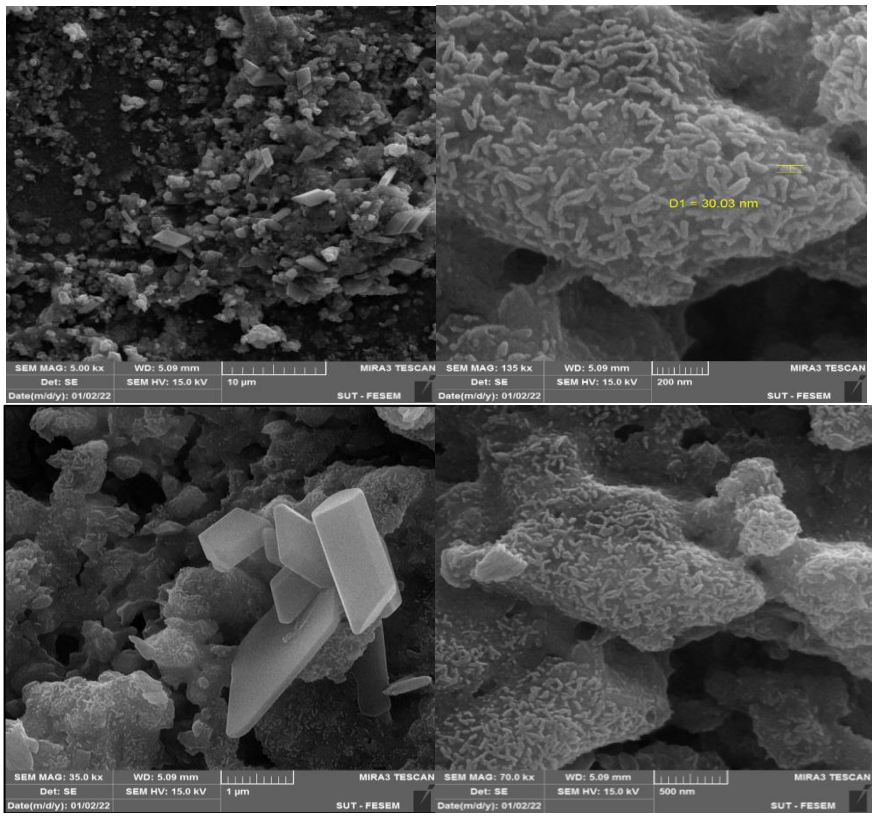

Figure 7. show the SEM image of (CuO-NPs)

Microscope with a transmission electron beam. (TEM)

A JEOL 2100Plus transmission electron microscopy (TEM) device operating at 200kV was used to capture the images. Adsorbent morphology was also characterized using TEM (Hassan et al., 2017; Naika et al., 2015). Figure (8) shows TEM images of copper (II) oxide, which clearly show a spherical morphology with particle sizes ranging from 40 to 80 nanometers.

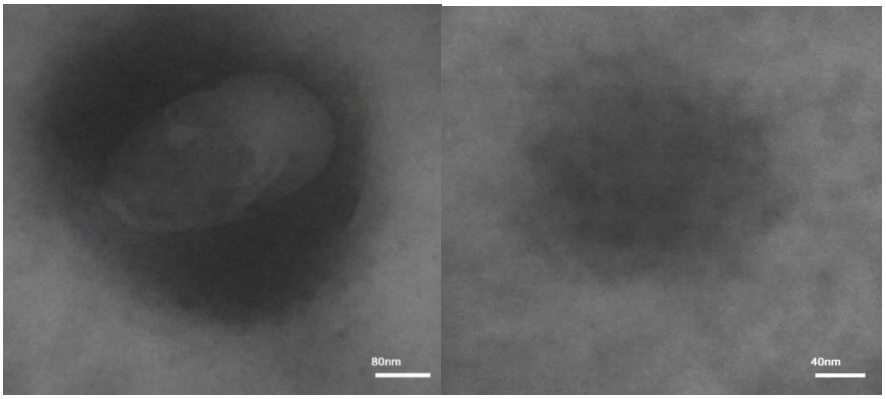

Figure 8. TEM images of synthesized (CuO-NPs)

Atomic force microscope

The AFM technique was used to investigate the surface morphology of the produced CuO NPs, as shown in Fig. 9. CuO NPs have a spherical form, as evidenced by AFM micrographs (Son et al., 2009). The nanoparticles have a lot of indents and abnormalities on their surfaces, as revealed by the topographic map. Rough surfaces have more active sites and a bigger surface area than smooth surfaces, so they can play a significant role in electrochemical activity. AFM was used to investigate the roughness of the CuO NPs powder's The Average grain size, roughness, and root mean square are(47, 0.470, and0.607) nm, respectively. As shown in Fig.9.

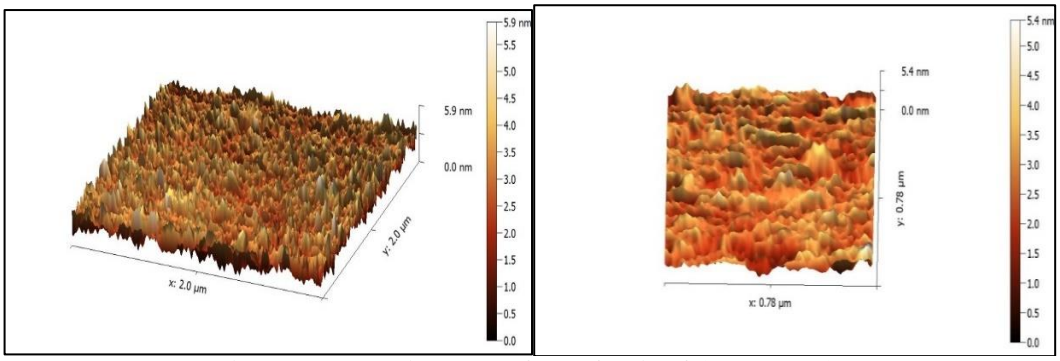

Figure 9. AFM images of synthesized (CuO-NPs).

The effect of contact time

The effect of contact time on the removal of [Pb (II) and Cr (II) ions from (CuO-NPs) was examined using contact durations of (15, 30, 45, 60, 75, 90, 105, and 120) minutes at 298 K, concentrations of 100 mg/L of each metal ion, and pH=7. Figure (10) Explain how the percentage of material removed changes as contact time increases. As can be observed, ion adsorption requires almost no time to reach equilibrium (90 min). Increasing percent removal at the start of contact time with Pb (II) and Cr (III) ions led in a long fall in the percentage removal of ions, despite the swift starting rate increase, according to the influence of contact time on ion removal using (CuO.NPs). Later stages are marked by a sluggish rate. It's possible that this is due to the adsorbent's plethora of adsorption destinations (Saeed et al., 2005). The underlying high adsorption rate could be because of particle trade followed by a sluggish substance response of the metal particles dynamic gatherings on the example (Maduabuchi, 2018), and the leftover empty surface locales are hard to be involved reason to shocking power. The metal particles need to cross farther and more profound into the pores experiencing a lot bigger opposition (Srivastava et al., 2006).

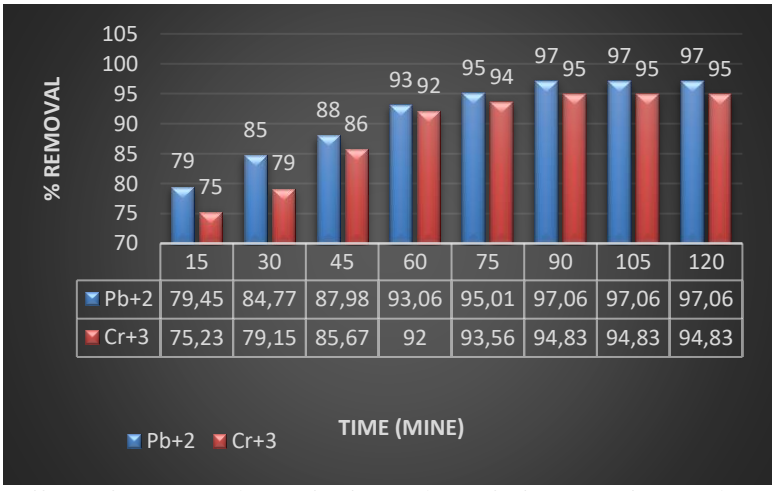

Figure 10. Effect of contact time of adsorption of Pb +2 and Cr+3 ions on (CuO - NPs)

Effect of adsorbent quantity on adsorption

The effect of the amount of adsorbent on the adsorption of Pb (II) and Cr (III) ions. Where the removal of Pb (II) and Cr(III) ions was studied on (CuO-NPs.) prepared by the green method using capers using different amounts of oxide (0.01, 0.05, 0.1, 0.15 and 0.20) g at 298 K, constant concentration of lead ions (100 PPm), pH 7 with a delivery time of 90 minutes. Effect of the quantity of adsorbents on the removal of lead (II) and Cr(III) ions Figure (11) shows the percentage of removal with each quantity covered. The amount of copper oxide nanoparticles can be observed, the removal of metal ions can be the bulk of the percentage of the refreshing removal in the place of adsorption, the optimum amount of adsorption can be an idea when removing Pb+2 and Cr+3 ions it is (0.1g) and after 0.1g,

Clearance rate is slightly increased. (Boujelben et al., 2009; El-Said et al., 2010; Han et al., 2006).

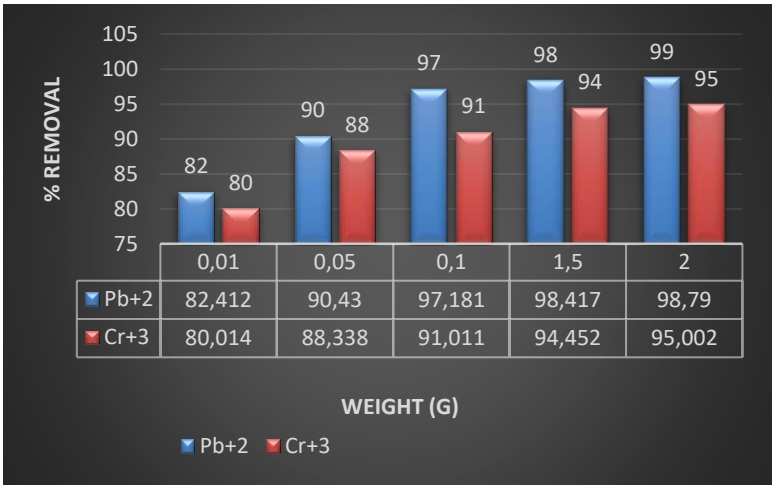

Figure 11. Effect of adsorbent quantity on adsorption:

The effect of temperature on adsorption is as follows

At different temperatures (298, 308, 318, 328, and 338 K) and pH 6.5, we explain the influence of temperature on the amount of absorption of Pb(II) and Cr(III) ions in at different temperatures and starting concentrations of 100 mg/L of Pb(II) and Cr(III) ions. At 60 minutes, the amount of adsorbent (0.1 g) and contact time remained consistent. The overall Pb (II) and Cr(III) ions adsorb in different forms on different surfaces. (.CuO-NPs) is shown in Figure (12), which shows that the percentage of removal decreases with the increase in temperature, this proves that the removal (Pb) and Cr ions on(.CuO-NPs) surface is exothermic, and the decrease in the adsorption rate inside the increase in temperature may weaken the interaction strength between Adsorption surface active sites and binary metal ions (Sheela et al., 2012).

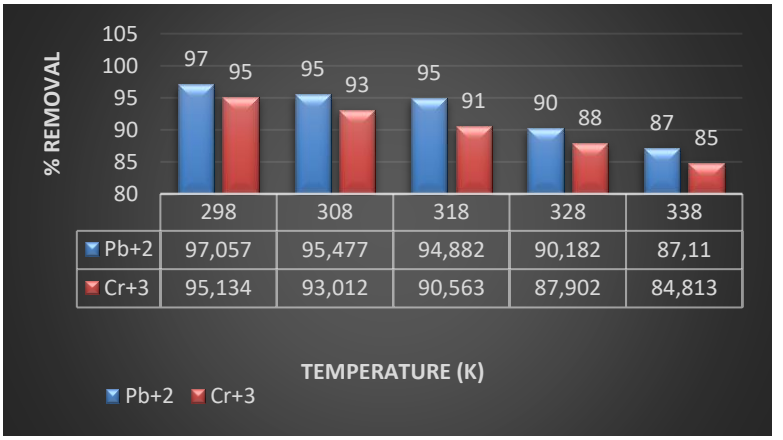

Figure 12. Effect of temperature on adsorption of Pb (II) and Cr (III) ions on (CuO-NPs)

Adsorption Effects of pH

At pH (3, 4, 5, 6, 7, 8, and 9) at 298 K, 60 min contact time, and adsorbent dose, the effect of pH on the percent removal of heavy metal ions from the copper oxide nanoparticle surface was examined (0.1 g). Figure 13 depicts the effects of pH on the elimination of Pb (II) and Cr (III). The removal of these metal ions was at its greatest at a pH of 7, as can be observed. When the pH climbs from 3 to 7, the absorption of heavy metal ions appears to increase. There is a strong electrostatic attraction between the positively charged surface of the copper oxide nanoparticles and the negatively charged surface of the copper oxide nanoparticles. repulsion at low pH. as well as cationic metals Furthermore, the increased concentration of H+ in the solution competes for adsorption sites with Pb (II). At pH of the binary system, the number of positively charged sites decreases and the number of negatively charged sites increases on the surfaces for reduced adsorptive of Pb (II) and Cr (III). Because of the rise in concentration of (OH-) ions in the aqueous solution, the copper oxide of the negatively charged surface site on the (CuO-NPs) the adsorption of Pb(II) and Cr(III) due to electrostatic attraction at pH values greater than (7) binary metals precipitated out.

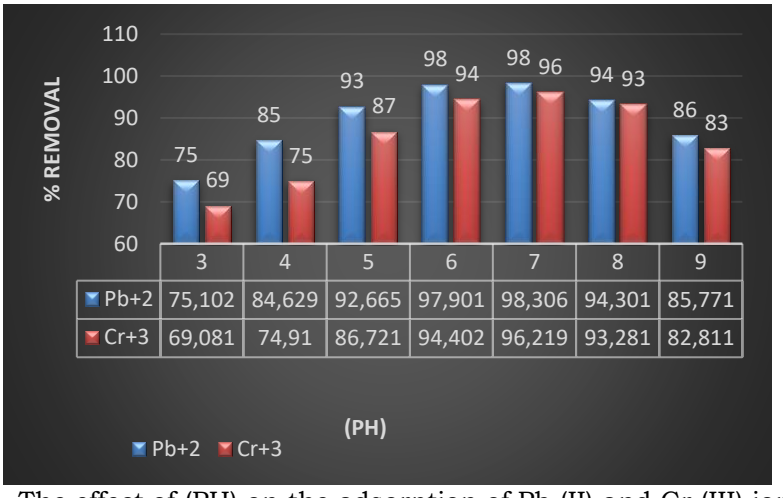

Figure 13. The effect of (PH) on the adsorption of Pb (II) and Cr (III) ions on the (CuO-NPs)

Initial concentration has the following effect

The adsorption of heavy metals (Pb II) and Cr (III) from an aqueous solution onto (.CuO-NPs) was first investigated under optimal circumstances, utilizing varying initial aqueous solution concentrations of (10, 20, 30, 40, 50, 60, and 70 PPm) for Pb (II) and Cr (III)ions. The results in Fig. (14) reveal that raising the initial concentration of Pb (II) and Cr (III) ions on the surface has minimal effect on removal (CuO-NPs). The minor decrease in % removal at higher concentrations could be ascribed to the copper oxide nanoparticles adsorbent's limited number of active sites, which become more saturated as metal ion concentrations rise, and removal of Pb (II) and Cr (III) particles on the (CuO-NPs) is high a direct result of

the little nanoparticle size and the high surface region that contains a great deal of dynamic adsorption locales which will be available (Jagung, 2011).

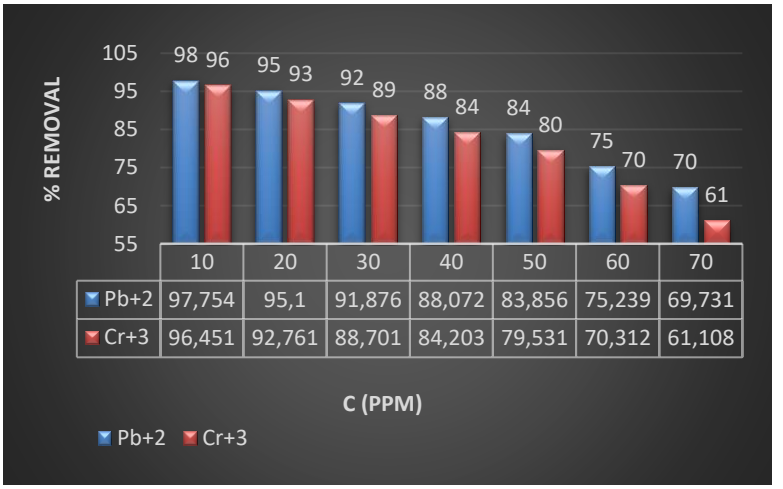

Figure 14. Effect of (starting concentration) on Pb (II) and Cr(III) ion adsorption (CuO-NPs)

Adsorption isotherms
Langmuir Equation

The Langmuir equation for adsorption of lead ions (II) and chromium (III) a dye was applied to the previously prepared adsorbent surface, which is copper oxide nanoparticles (CuO -NPs) prepared by the green method at a temperature of (298 K) and from the slope and intercept we plot (Ce/Qe vs. Ce) As shown in the figure (13) then the Langmuir constants were extracted as shown in the table (2) according to the following equation.

$$\frac{Ce}{Qe} = \frac{1}{Qmax.k1} + \frac{Ce}{Qmax}$$

The slope and cut-off of the linear connection between Ce against Ce/Qe were used to get the values of Qmax and Kl.

Friendlich isotherm

The linear Friendlich equation was utilized to apply the adsorbents' practical adsorption findings to the utilized adsorbent surfaces.

$$LnQe = LnKf + \frac{1}{n} LnCe$$

The slope and cutoff linear connection between LnQe and LnCe were used to calculate the Freundlich constants n and Kf, as well as the value of the correlation coefficient R2 for the adsorption process.

Table 2
Freundlich and Langmuir constants on the surface of (CuO-Nps)

Adsorbent	Langmuir			Freundilch		
	R^2	$Q_{max\times10^3}$	K_l	R^2	n	K_f
Pb+2	0.9857	769.2	0.0296	0.9965	1.268	27.207
Cr+3	0.9975	1428.5	0.0099	0.9939	1.099	15.113

The results in Table (2) show that the Langmuir adsorption equation, which produced high linear correlation coefficients between the diverse adsorption processes on the constructed adsorbent surfaces, applies to them in part (0.9986-0.9857). Also, the Friendlich equation applies to it, where it gives linear correlation coefficients between (0.99655-0.9939). From the results, we find that the values of (n>1), which represents the intensity of adsorption, which indicates that the adsorption that occurs is physical adsorption (Al-abady et al., 2019). This is what happened with us upon the adsorption of the two ions shown in our study

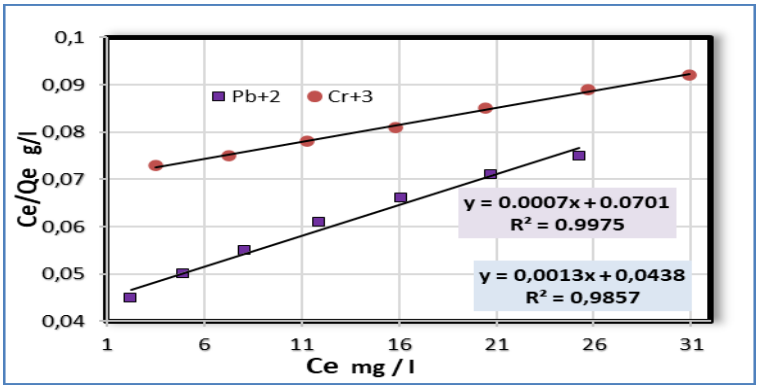

Figure 15. Langmuir isotherm to remove (Pb+2), (Cr+3) on the surface of (CuO-NPs)

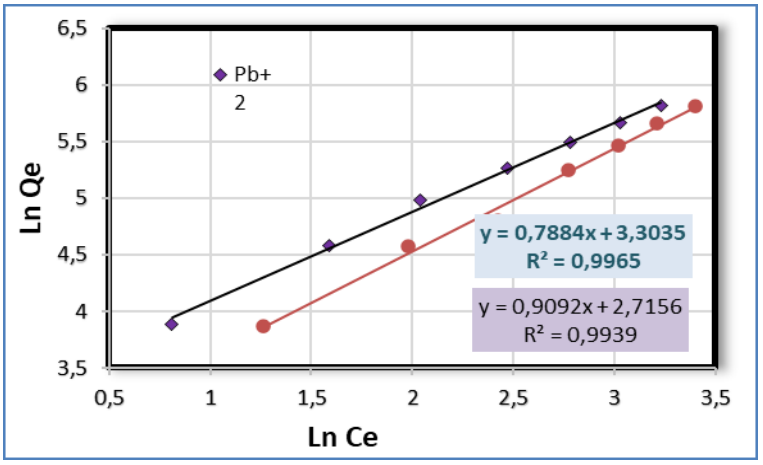

Figure 16. Freundlich isotherm to remove (Pb+2), (Cr+3) on the surface of CuO-NPs

Thermodynamics

The thermodynamic functions of adsorption were calculated for (Pb + 2) and (Cr + 3). Using nanoparticles of copper oxide prepared by the green method. The content values for adsorption and adsorption entropy (ΔS) were calculated using the Vant Hoff equation (Mohammed et al., 2020).

$$LnK = \frac{\Delta S}{R} - \frac{\Delta H}{RT} \quad , \quad K = \frac{Qe}{Ce}$$

The slope and cut-offs of the straight line equation were calculated from the graph of Ln k vs. 1/T, and the values of ΔH and ΔS were calculated from the slope and cut-offs of the straight line equation, respectively. Gibbs' mathematical equation was also used to compute the value of the free energy G.

$$\Delta G = \Delta H - T \cdot \Delta S$$

Table (6) show that the heat of adsorption (ΔH) is positive, indicating that all adsorption processes are endothermic, and that all values were less than (40 kg/mol), that adsorbent surfaces is physical. 23 Negative (ΔG) values suggest that adsorption processes happen on spontaneously. The positive values of (ΔS) imply that the adsorbed molecules are less regular on the adsorbing surface than they are in the solution.

Table 3
Thermodynamic functions of adsorption on the surface of (CuO-NPs)

T_K	Pb^{+2}			Cr^{+3}		
	ΔG	ΔH	ΔS	ΔG	ΔH	ΔS
298	-6.96			-6.26		
308	-6.04	-33.4	-86.7	-4.91	-30.1	-78.9
318	-5.89			-4.15		
328	-4.14			-3.51		
338	-3.42			-2.89		

The obtained results indicate that the enthalpy values of adsorption (ΔH) were negative with both lead (II) ion and chromium (III) ion and therefore the adsorption processes are exothermic and that all values were less than (40 kj / mol), which is an indication of The adsorption processes on the characteristic surfaces are of a physical nature (Mohammed et al., 2020). The values of free energy ΔG indicate that all processes occur spontaneously because all values were negative. While the resulting values of (ΔS) for the two adsorbed ions, their values were negative, and this is evidence that the processes are less random, which proves that the adsorbed molecules are more regular on the adsorbent surfaces.

Conclusion

Capparis Spinosa leaves extract and Cu (NO3)2 metal salt is used to synthesize copper nanoparticles, which is a simple and environmentally friendly process. This method has numerous benefits, including economic viability, ease of scaling up, and reduced time consumption. Copper nanoparticles prepared in this way can be used as active surfaces to separate and remove heavy elements like chromium and lead from polluted water.

Acknowledgement

The authors would like to thank Department of Chemistry, College of Education for Pure Sciences, University of Anbar, Ramadi, Iraq and Department of Chemistry, College of Science, Al-Mustansiriyah University, Baghdad, Iraq.

References

Aguilera, A., Klemenčič, M., Sueldo, D. J., Rzymski, P., Giannuzzi, L., & Martin, M. V., 2021. Cell Death in Cyanobacteria: Current Understanding and Recommendations for a Consensus on Its Nomenclature. Frontiers in microbiology, 12, 631654. https://doi.org/10.3389/fmicb.2021.631654.

Ali H., Khan E., Sajad M.A., 2013. Phytoremediation of heavy metals—Concepts and applications. Chemosphere, 91, 869–881.

Damayanti, I. A. M., Indrayoni, P., Antari, N. W. S., & Padmiswari, A. A. I. M. (2021). Effectiveness of Averrhoa bilimbi leaf extract on spermatogenic cells of mice (Mus Musculus L.) hyperglycemia. *International Journal of Health & Medical Sciences*, *4*(2), 273-279. https://doi.org/10.21744/ijhms.v4n2.1747

El-SheekhMostafa, HamoudaRagaa, Adnan A. Nizam, 2013. Biodegradation of crude oil by Scenedesmus obliquus and Chlorella vulgaris growing under heterotrophic conditions. International Biodeterioration & Biodegradation 82:67–72.

Endalkachew Sahle-Demessie, AshrafAly Hassan, AmroEl Badawy, 2019. Bio-desalination of brackish and seawater using halophytic algae. Desalination, Vol. 465, pp. 104-113**.**

Guiry M. D. and Guiry G. M. (2018): AlgaeBase.– World-wide electronic publication, National University of Ireland, Galway, URL: http://www.algaebase.org.

Liu, S.-Y.; Zhao, R.-Z.; Qiu, X.-C.; Guo, Q. Optimization Analysis to Evaluate the Relationships between Different Ion Concentrations and Prymnesium parvum Growth Rate. Water 2022, 14, 928. https://doi.org/ 10.3390/w14060928.

Melero-Jiménez Ignacio J., Bañares-España Elena, García-Sánchez María J., Flores-Moya Antonio, 2022. Changes in the growth rate of *Chlamydomonas reinhardtii* under long-term selection by temperature and salinity: Acclimation *vs*. evolution. Science of the total environment, Vol. 822, 153467.

Muhlsteinova R., Hauer T., De Ley P. & Pietrasiak N., 2018. Seeking the true *Oscillatoria*: a quest for a reliable phylogenetic and taxonomic reference point. Preslia 90: pp.151–169.

Nadi, E., and Hosseiny, E., 2019. SIMPLE SIMULATION MODEL FOR BIOLOGICAL DESALINATION BY ALGAE. World Journal of Engineering Research and Technology, Vol. 5, Issue 1, 299316.

Nandagopal P., Steven A.N., Chan L.-W., Rahmat Z., Jamaluddin H., Mohd Noh N.I., 2021. Bioactive Metabolites Produced by Cyanobacteria for Growth Adaptation and Their Pharmacological Properties. Biology, 10, 1061. https://doi.org/ 10.3390/biology10101061.

Nurul Salma Adenan, Fatimah Md. Yusoff and Mohamed Shariff, 2013. Effect of Salinity and Temperature on the Growth of Diatoms and Green Algae. *Journal of Fisheries and Aquatic Science, 8: 397-404.*

Saeid Aghahossein Shirazia, Jalal Rastegaryb, Masoud Aghajanic, Abbas Ghassemi, 2018. Simultaneous biomass production and water desalination concentrate treatmentby using microalgae. Desalination and Water Treatment, 135, pp.101–107.

Shah, S.M.U., Che Radziah, C., Ibrahim, S., 2014. Effects of photoperiod, salinity, and pH on cell growth and lipid content of *Pavlova lutheri*. *Ann Microbiol*, 64, 157–164. https://doi.org/10.1007/s13213-013-0645-6.

Shaila Hiremath and Pratima Mathad, 2008. Amelioration of Salinity-Induced Metabolic Changes in Oscillatoria willei by Gypsum. J. Algal Biomass Utln. 3 (1): 1 – 4.

Silveira SB., and Odebrecht C., 2019. Effects of Salinity and Temperature on the Growth, Toxin Production, and Akinete Germination of the Cyanobacterium Nodularia spumigena. Front. Mar. Sci. 6:339. doi: 10.3389/fmars.2019.00339

Suryasa, I. W., Rodríguez-Gámez, M., & Koldoris, T. (2021). Health and treatment of diabetes mellitus. *International Journal of Health Sciences*, *5*(1), i-v. https://doi.org/10.53730/ijhs.v5n1.2864

Valipour A., Hamnabard N., Woo K.S., Ahn Y.H., 2014. Performance of high-rate constructed phytoremediation process with attached growth for domestic wastewater treatment: Effect of high TDS and Cu. J. Environ. Manag., 145, 108.

Wangwibulkit Somchai, Limsuwan Chalor, and Chuchird Niti, 2008. Effects of Salinity and pH on the Growth of Blue-Green Algae, Oscillatoria sp. and Microcystis sp., Isolated from Pacific White Shrimp (Litopenaeus vannamei) Ponds. Journal of fisheries and environment, Vol. 32 No. 1.